PCCP

PAPER

View Article Online
View Journal | View Issue

Cite this: *Phys. Chem. Chem. Phys.*, 2017, **19**, 31274

Explaining the symmetry breaking observed in the endofullerenes $H_2@C_{60}$, $HF@C_{60}$, and $H_2O@C_{60}$†

Peter M. Felker, *[a] Vojtěch Vlček,[a] Isaac Hietanen,[b] Stephen FitzGerald,[b] Daniel Neuhauser[a] and Zlatko Bačić *[cd]

Received 5th September 2017,
Accepted 2nd November 2017

DOI: 10.1039/c7cp06062a

rsc.li/pccp

Symmetry breaking has been recently observed in the endofullerenes M@C_{60} (M = H_2, HF, H_2O), manifesting in the splittings of the three-fold degenerate ground states of the endohedral *ortho*-H_2, *ortho*-H_2O and the j = 1 level of HF. The nature of the interaction causing the symmetry breaking is established in this study. A fragment of the solid C_{60} is considered, comprised of the central C_{60} molecule surrounded by twelve nearest-neighbor (NN) C_{60} molecules. The fullerenes have either P (major) or H (minor) orientational orderings, and are assumed to be rigid with I_h symmetry. Only the central C_{60} is occupied by the guest molecule M, while the NN fullerenes are all empty. The key proposition of the study is that the electrostatic interactions between the charge densities on the NN C_{60} molecules and that on M inside the central C_{60} give rise to the symmetry breaking responsible for the measured level splittings. Using this model, the M@C_{60} level splittings of interest are calculated variationally and using perturbation theory, for both the P and H orientations. Those obtained for the dominant P orientation are in excellent agreement with the experimental results, with respect to the splitting magnitudes and patterns, for all three M@C_{60} systems considered, pointing strongly to the quadrupolar M–NN interactions as the main cause of the symmetry breaking. The level splittings calculated for the H orientation are about 30 times smaller than the ones in the P orientation.

1 Introduction

Light-molecule endofullerenes are a class of supramolecular systems where a light molecule, *e.g.*, H_2, H_2O, or HF, is encapsulated inside a fullerene cage.[1] Their iconic representative is $H_2@C_{60}$, where the H_2 molecule is trapped in the nanoscale cavity of C_{60}. This entrapment was accomplished in 2005 by Komatsu and co-workers[2,3] using the approach known as molecular surgery,[4–6] whereby through a series of organic reactions the fullerene cage is first opened, the guest molecule is inserted, and the cage is then closed with the molecule permanently in its interior. In 2011, the molecular surgery technique was utilized to achieve another milestone, the synthesis of $H_2O@C_{60}$.[7] Most recently, the same approach led to the preparation of $HF@C_{60}$.[8] As a result of these synthetic feats, $H_2@C_{60}$, $H_2O@C_{60}$, and $HF@C_{60}$ have become available in macroscopic quantities, enabling a wide range of spectroscopic studies of their fundamental properties.

The most distinguishing feature of the light-molecule endofullerenes M@C_{60} (M = H_2, H_2O, HF) is the highly quantum nature of the dynamics of the guest molecule, particularly evident for the low temperatures at which the spectroscopic measurements on M@C_{60} are usually performed (typically ranging from 1.5 K to about 30 K). Owing to the combination of its tight confinement inside C_{60} and low molecular mass, the translational center-of-mass (c.m.) degrees of freedom of M are quantized and the eigenstates are well separated in energy relative to kT (where k is the Boltzmann constant). The same holds for the quantized rotational states due to the large rotational constants of these molecules. Furthermore, the confining potential of the C_{60} cage couples the translational and rotational motions of M, giving rise to a sparse translation–rotation (TR) (or "rattling") energy level structure.

The quantum features of the TR dynamics are enhanced further when M has two symmetrically equivalent ^{1}H nuclei (H_2 and H_2O) that, having nuclear spin 1/2, are fermions. According to the Pauli principle, the total molecular wave function of M, its spatial and spin components, must be antisymmetric with respect to the exchange of the two fermions. This requirement can be met only for certain combinations of the spin and spatial quantum states, resulting in nuclear spin isomers, denoted *para* and *ortho*, of both

[a] *Department of Chemistry and Biochemistry, University of California, Los Angeles, CA 90095-1569, USA. E-mail: felker@chem.ucla.edu*
[b] *Department of Physics and Astronomy, Oberlin College, Oberlin, OH 44074, USA*
[c] *Department of Chemistry, New York University, New York, NY, 10003, USA. E-mail: zlatko.bacic@nyu.edu*
[d] *NYU-ECNU Center for Computational Chemistry at NYU Shanghai, 3663 Zhongshan Road North, Shanghai, 200062, China*

† Electronic supplementary information (ESI) available. See DOI: 10.1039/c7cp06062a

H_2 and H_2O, with total nuclear spins $I = 0$ and 1, respectively. For *para*-H_2, only even rotational quantum numbers j are allowed ($j = 0, 2, \ldots$), while *ortho*-H_2 can only have odd rotational quantum numbers $j = 1, 3, \ldots$. The rotational states of H_2O are conventionally labelled with the asymmetric top quantum numbers $j_{k_a k_c}$; for *para*-H_2O, $k_a + k_c$ has even parity, while for *ortho*-H_2O, $k_a + k_c$ has odd parity.[9] These restrictions on the rotational quantum numbers of the spin isomers of H_2 and H_2O make their already sparse TR level structure even sparser.

The quantum TR dynamics of H_2 and its isotopologues in C_{60}[10] has received a great deal of scrutiny from both theoretical[11–17] and experimental studies, primarily inelastic neutron scattering (INS)[18–21] and infrared (IR).[14,22–24] Its salient features were established in a series of theoretical investigations.[11–15] The translational eigenstates can be assigned with the principal quantum number $n = 0, 1, 2, \ldots$, of the 3D isotropic harmonic oscillator (HO) and its orbital angular momentum quantum number $l = n, n - 2, \ldots, 1$ or 0, for odd and even n, respectively. The quantum numbers $j = 0, 1, 2, \ldots$, of a linear rigid rotor can be used for assigning the rotational energy levels of the caged H_2. The TR states of $H_2@C_{60}$ with simultaneous translational and rotational excitation exhibit vectorial coupling between the orbital angular momentum l associated with the translational c.m. motion of H_2 and the rotational angular momentum j to give the total angular momentum with the quantum numbers $\lambda = l + j, l + j - 1, \ldots, |l - j|$, and the degeneracy of $2\lambda + 1$.[11] This coupling manifests in the splitting of such TR eigenstates into as many closely spaced levels as there are values of λ, each having the degeneracy $2\lambda + 1$.[11,12] The TR energy level structure of $H_2O@C_{60}$, determined by means of rigorous quantum 6D calculations,[25] bears many similarities to that of $H_2@C_{60}$, including the coupling of the orbital and rotational angular momenta.

The link between theory and experiment for $H_2@C_{60}$ was strengthened by the development of the methodology for rigorous quantum calculation of the INS spectra of a hydrogen molecule confined inside a nanocavity.[26–28] Using this methodology, highly realistic simulations of the INS spectra of H_2 and HD in C_{60} have been performed.[16,17,29] They led to the unexpected discovery of a selection rule in the INS spectroscopy of H_2[17] and HD[16] confined inside near-spherical nanocavities such as that of C_{60}. This selection rule, the first ever to be established for the INS spectroscopy of discrete molecular compounds, was soon confirmed experimentally[29] and generalized.[30,31]

In all of the above studies of $H_2@C_{60}$, theoretical and experimental, it was assumed, explicitly or tacitly, that the endohedral H_2 was inside a cage with I_h symmetry, which is the symmetry of an isolated C_{60} molecule. In such an environment, the $j = 1$ ground state of *ortho*-H_2 maintains the three-fold degeneracy that it has in the gas phase. However, beginning in 2009, evidence has emerged from several lines of investigation of solid $H_2@C_{60}$ employing different experimental techniques that this is not strictly true. From the specific heat anomaly observed at low temperatures (below 4 K) for $H_2@C_{60}$, Kohama *et al.*[32] deduced that the $j = 1$ triplet of *ortho*-H_2 is split, by about 1.13 cm^{-1}, into a lower-energy state that is non-degenerate and a doubly degenerate higher-energy state. The lifting of the $j = 1$ degeneracy signals symmetry breaking of the environment felt by the encapsulated H_2. The possibilities regarding the origins of such symmetry lowering will be discussed shortly.

Another piece of evidence for the splitting of the ground state of *ortho*-H_2 is provided by the low-temperature (6 K) IR absorption spectra of the $H_2@C_{60}$ powder sample.[14,24] Figuring prominently in them is the set of Q(1) transitions from the ground state of *ortho*-H_2 to three $n = 1$, $j = 1$ sublevels corresponding to $\lambda = 1$, 2, 0, respectively, in the order of increasing energies. The $\lambda = 0$ band is split by about 1 cm^{-1}, reflecting directly the splitting of the initial *ortho*-H_2 $j = 1$ ground state.

The symmetry breaking in $H_2@C_{60}$ was investigated by INS as well,[33] by studying the temperature dependence of the line (its shape, width, and peak position) corresponding to the transitions from the ground state of *ortho*-H_2 to the ground state of *para*-H_2 (neutron energy gain), in the range 0.06–35 K. From the analysis of the data it emerged that the $j = 1$ triplet of *ortho*-H_2 is split into a lower-energy level that is non-degenerate and a higher-energy doubly degenerate level, separated by 1.09 cm^{-1}. Thus, three totally independent experimental techniques have shown that the ground state of *ortho*-$H_2@C_{60}$ exhibits 1 : 2 splitting of about 1 cm^{-1}.

Symmetry breaking has been observed also in $H_2O@C_{60}$ and $HF@C_{60}$, where the guest molecules, H_2O and HF respectively, have permanent electric dipoles. The initial INS and nuclear magnetic resonance (NMR) spectra of solid $H_2O@C_{60}$[34] revealed the splitting of the three-fold degenerate 1_{01} ground state of *ortho*-H_2O into a non-degenerate lower-energy state and a doubly degenerate higher-energy state, by about 4.8 cm^{-1}. The subsequent in-depth INS investigation using a highly purified sample of $H_2O@C_{60}$ confirmed this splitting pattern, and yielded the splitting of 4.19 cm^{-1}.[35,36] For $HF@C_{60}$, the symmetry breaking manifested as the splitting of the $j = 0 \rightarrow j = 1$ transition by 3.9 cm^{-1}, in the far- and mid-IR spectra of the polycrystalline sample.[8]

The above suggests that symmetry breaking is a rule, rather than an exception, for light-molecule endofullerenes in the crystalline solid state, regardless of whether the endohedral molecules have a permanent electric dipole (H_2O, HF) or not (H_2). But, what is its origin, or mechanism? A couple of possibilities has been suggested. One is that the breakdown of the icosahedral symmetry is caused by the distortion of the host C_{60} cage due to the interaction with the guest molecule in its interior.[8,33–35] An alternative is that the symmetry breaking arises from inter-cage interactions and, when the guest molecules have a permanent electric dipole, also from dipolar interactions between the guest molecules in neighboring C_{60} cages, potentially leading to the alignment of their dipoles.[34,35] It is possible, of course, that both intra- and inter-cage interactions contribute to the symmetry reduction. The problem with these and related proposals is that attempting to validate them by comparison with the experimental findings would require very difficult high-dimensional quantum calculations that have not been performed so far.

In the experimental studies of the symmetry breaking in $H_2@C_{60}(s)$[32,33] it was postulated that this phenomenon may be

linked to the orientational ordering of C_{60} molecules in the solid at low temperatures. Above 260 K, the C_{60} molecules rotate almost freely and independently of one another,[37,38] and the solid has face centered cubic (fcc) symmetry. However, at temperatures below 90 K, the C_{60} rotations are entirely frozen,[38] and the crystal structure is now simple cubic (sc, $Pa\bar{3}$). The C_{60} molecules are locked in, and coexist in, two orientationally optimized configurations of neighboring units. In the dominant one, referred to as the P orientation, associated with the global minimum of the inter-cage potential, the electron-rich double bonds shared by two hexagons (denoted 6:6) of one C_{60} unit face directly the electron-poor pentagons of the neighboring cages.[38,39] Each C_{60} unit has six electron-rich 6:6 bonds and six electron-deficient pentagons facing its twelve nearest neighbors. Thus, this configuration is stabilized by optimizing the electrostatic interactions between the neighboring C_{60} units.[38,39] The slightly higher local minimum on the inter-cage potential corresponds to what is denoted as the H orientation, where electron-rich 6:6 bonds of one C_{60} are now immediately adjacent to the electron-poor hexagonal faces of the neighboring units.[38] Therefore, the H orientation is also stabilized by the inter-cage electrostatic interactions. Below 90 K, and at ambient pressure, the relative proportion of molecules in the P and H orientations is 5:1.[38] At the intermediate temperatures below 260 K and above $\sim$90 K, the C_{60} molecules perform a ratcheting motion, thermally activated jumps between the inequivalent P and H orientations and the corresponding 60 symmetry-related orientations.

What makes the P and H orientations in C_{60}(s) relevant for the symmetry breaking is that in both the point-group symmetry of the environment at the center of a C_{60} cage is S_6,[32,33] which in principle can split the three-fold degeneracy of the ground states of *ortho*-H_2, *ortho*-H_2O, and the $j = 1$ state of HF into a non-degenerate and a doubly degenerate state. However, for this symmetry lowering to be significant, and its consequences observable, the guest molecule inside one C_{60} must have appreciable interactions with the nearest-neighbor units, not just its own cage. But so far, the nature of this crucial interaction has remained totally unresolved. Moreover, in the case of dipolar fullerenes, $H_2O@C_{60}$ and $HF@C_{60}$, an open question is how much, if anything, the dipole–dipole interactions between the guest molecules contribute to the symmetry breaking. Not surprisingly given this state of affairs, no attempt has been made to calculate the symmetry-breaking induced splittings and compare them with experiment.

In order to address the above issues quantitatively, in this paper we resort to what in view of the complexity of the problem is conceptually a rather minimalistic approach. Nevertheless, the approach is intricate formally and computationally demanding – and proves to be remarkably accurate. We consider a fragment of C_{60}(s) where the central cage is surrounded by the twelve nearest-neighbor cages, with all the cages in either P or H orientations. For both, the site symmetry at the center of the central C_{60} is S_6. Only the central cage contains the guest molecule M (M = H_2, H_2O, HF), while all other cages are empty. The fragment as a whole and the individual C_{60} cages are treated as rigid, and the cages are assumed to have icosahedral symmetry.

In our preliminary quantum-bound state calculations the interaction between M, H_2 or H_2O, and the 13-C_{60} fragment was represented as a sum of pairwise-additive Lennard-Jones (LJ) potentials between the sites on M and all 780 C atoms of the fragment. The LJ parameters were taken from our earlier studies of $H_2@C_{60}$[17] and $H_2O@C_{60}$,[25] respectively. These calculations yielded splittings of the ground states of *ortho*-H_2 and *ortho*-H_2O orders of magnitude smaller than the experimental values, demonstrating that LJ interactions contribute negligibly to the symmetry breaking. This was not particularly surprising given the short-range nature of the LJ potentials that effectively limits their significance to the interaction of M with the central host cage that, by assumption, has I_h symmetry and cannot cause splittings of the rotational levels of interest.

This has led us to consider the possibility, central to this paper, that the electrostatic interaction between the charge density on the twelve neighboring cages and that on M encapsulated in the central cage is the main cause of the symmetry breaking. The reasoning behind this key conjecture is that since the electrostatic interactions between the anisotropic electron density distributions on the C_{60} cages are responsible for the existence of the P and H orientations in the first place, and have long-range character, they also have the potential to make a major contribution to the symmetry breaking in endohedral fullerene solids.

For this electrostatic-interaction model, and utilizing the fragment electronic charge density distribution from the DFT calculations for a single C_{60}, the splittings of the desired TR levels of M are calculated by means of both variational calculations and perturbation theory (PT) for the P and H orientations; they are found to differ greatly for the two orientations. As discussed later in the paper, the level splittings for the P orientation from the variational and PT calculations are in excellent agreement with the corresponding experimental values for all three endofullerenes (while those obtained for the H orientation are negligibly small). This is a most remarkable result, in view of what the model employed does not include: (a) distortion of the central cage geometry due to the presence of M, and (b) interactions between the guest molecules in the neighboring cages. This approach was initially conceived and developed with $H_2@C_{60}$ in mind, for which neither of these limitations was expected to introduce a significant error in the calculated level splittings, given that both the H_2–cage and H_2–H_2 intermolecular interactions are very weak, the latter because of the large distance, about 19 Bohr,[40] between the centers of the nearest-neighbor cages in solid C_{60}. However, it was by no means obvious that the model would work so well in the case of $H_2O@C_{60}$ and $HF@C_{60}$. The permanent electric dipole on both endohedral molecules has been expected to play a significant role in the symmetry breaking through either cage distortion or the cooperative dipolar alignment, or both.[8,34,35]

The paper is organized as follows. In Section 2, the theory for calculating the splittings of the TR levels of endohedral molecules inside the cages of C_{60}(s) is presented. Theoretical results and their comparison with experimental values are presented and discussed in Section 3. Conclusions are given in Section 4.

2 Theory

2.1 Hamiltonian

For the electrostatic-interaction model introduced in Section 1, the TR Hamiltonian of M confined inside the central cage of the thirteen-cage fragment of M@C_{60}(s) can be written as

$$\hat{H} = \hat{T}(\mathbf{R},\omega) + V_{\mathrm{M}-\mathrm{C}_{60}}(\mathbf{R},\omega) + V_{\mathrm{ES}}(\mathbf{R},\omega). \quad (1)$$

In eqn (1), $\hat{T}$ is the kinetic-energy operator corresponding to the TR motions of rigid M, $V_{\mathrm{M}-\mathrm{C}_{60}}$ is the intermolecular potential energy surface (PES) for M in the host C_{60} (5D for H_2 and 6D for H_2O), and V_{ES} is the electrostatic interaction between the charge density distribution on M and that on the twelve nearest-neighbor (NN) C_{60} cages that surround the central cage. In the case of H_2 and H_2O, $V_{\mathrm{M}-\mathrm{C}_{60}}$ is defined in our previous studies of H_2@C_{60}[17] and H_2O@C_{60},[25] respectively. Both PESs are constructed as sums of pairwise-additive LJ potentials between the sites on M and the 60 C atoms of the cage. No PES is presently available for HF@C_{60}. It should be noted that the charge density on M interacts also with that of its host C_{60} cage, but this interaction is already effectively accounted for by the parametrization of the LJ potentials comprising $V_{\mathrm{M}-\mathrm{C}_{60}}$ in eqn (1).

The coordinates **R** and ω fix the c.m. position and orientation, respectively, of M with respect to (w.r.t.) a space-fixed (SF) cartesian system. The latter has its origin at the center of the central C_{60} cage and is oriented in such a way that the C_3 symmetry axis of the thirteen-cage fragment is along the (1,1,1) direction. **R** is the position vector from the SF origin to the c.m. of M. ω represents the collection of two (M = H_2 and HF) or three (M = H_2O) angles that define the orientation of a body-fixed (BF) axis system affixed to M relative to the SF frame. (Details pertaining to $\hat{T}$ and the geometries of the M and of the thirteen-cage fragment are given in the ESI.†)

Now V_{ES}, the M/NN–cage electrostatic interaction, arises from two spatially separated charge density distributions. Given this, one can write it as a sum over products of spherical multipoles (*e.g.*, see eqn (5), p. 247 of Zare[41])

$$V_{\mathrm{ES}} = \sum_{l=0}^{\infty}\sum_{m=-l}^{l}(-1)^m I_{-m}^{(l)} Q_m^{(l)}, \quad (2)$$

where the ''interior'' moments, $I_m^{(l)}$, relate to the charge-density distribution on the NN cages

$$I_m^{(l)} \equiv \int \frac{\rho_{\mathrm{NN}}(\mathbf{r}) C_m^{(l)}(\hat{r})}{r^{l+1}} \mathrm{d}\mathbf{r}, \quad (3)$$

and the ''molecular'' moments $Q_m^{(l)}$ relate to the charge-density distribution on M

$$Q_m^{(l)} \equiv \int \rho_{\mathrm{M}}(\mathbf{r}) r^l C_m^{(l)}(\hat{r}) \mathrm{d}\mathbf{r}. \quad (4)$$

In eqn (3) and (4) $\mathbf{r} = r\hat{r}$ is the position vector pointing from the origin of the SF frame to some point in space, $C_m^{(l)}(\hat{r})$ are solid harmonics dependent on the polar and azimuthal angles defining the orientation of the unit vector $\hat{r}$ w.r.t. the SF axes, $\rho_{\mathrm{NN}}(\mathbf{r})$ is the charge-density function of the NN cages, and $\rho_{\mathrm{M}}(\mathbf{r})$ is that of M.

The $l = 0$ term in eqn (2) is zero because the charge neutrality of M renders the $l = 0$ molecular moment zero. All odd-l terms in eqn (2) are also zero. This follows from the inversion symmetry of ρ_{NN}

$$\rho_{\mathrm{NN}}(-\mathbf{r}) = \rho_{\mathrm{NN}}(\mathbf{r}), \quad (5)$$

a consequence of the S_6 symmetry of the C_{60} fragment. The upshot is that the leading terms in V_{ES} are those that correspond to $l = 2$ (the quadrupole terms) and that the next lowest-order contributions come from $l = 4$. Given that $I_m^{(l)}$ fall off with l much more rapidly than the $Q_m^{(l)}$ increase with l (the relevant $1/r^{l+1}$ factors in eqn (3) correspond to $r \geq 7$ Bohr whereas the relevant r^l factors in eqn (4) correspond to $r \leq 2$ Bohr), truncation of V_{ES} at the quadrupole terms is an excellent approximation:

$$V_{\mathrm{ES}} \simeq V_{\mathrm{quad}}(\mathbf{R},\omega) \equiv \sum_{m=-2}^{2}(-1)^m I_{-m}^{(2)} Q_m^{(2)}(\mathbf{R},\omega). \quad (6)$$

$I_m^{(l)}$ for $l = 2$ are the components of the ''electric field gradient tensor.''[41] Note that these depend solely on the cage-fragment geometry and do not depend on either the TR coordinates of M or its chemical identity (H_2, HF, or H_2O). $Q_m^{(2)}$ constitute the SF components of the M's quadrupole-moment tensor. These do depend on **R** and ω, as well as on the BF components of the M's quadrupole.

The key proposition of this paper is that V_{quad} in eqn (6) can account for the observed manifestations of symmetry breaking in all three of the M@C_{60} species considered here. In the following, we will refer to this as the quadrupolar model.

2.2 The electric field gradient tensor, $I_m^{(2)}$

$I_m^{(2)}$ depend on $\rho_{\mathrm{NN}}(\mathbf{r})$, which can be determined if one knows the positions of the twelve NN cages about the central cage and the charge-density function of an individual C_{60} cage. (We make the assumption that the charge-density function of a C_{60} cage in the solid can be reasonably approximated by that of isolated C_{60}.)

2.2.1 C_{60} cage positions. The positions of the NN cages about the central cage are available from the experimentally determined crystallographic parameters for C_{60}(s),[42,43] if one makes the assumption (verified experimentally for H_2O@C_{60}[44]) that the unit-cell geometries found for C_{60}(s) also apply to the M@C_{60}(s) species. As stated in the Introduction, the prevalent form (85% for C_{60}(s)) at atmospheric pressure and low temperature has the P orientation. It consists of closest-contact interactions between the central cage and each of the NN cages in which a 6:6 bond on one cage is positioned directly above a pentagonal ring on the other. In six of these interactions the central-cage moiety participates *via* a 6:6 bond, and in the other six it participates *via* a pentagonal ring. We label the six NN cages involved in the former interactions ''equatorial'' and the six involved in the latter ''axial'' – see Fig. 1. The H orientation is similar to the P orientation except that the

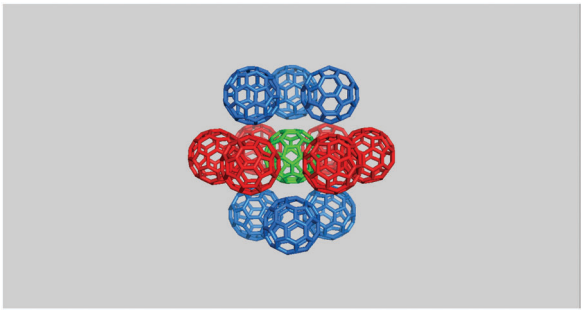

Fig. 1 The 13-cage unit of the P orientation of C_{60}(s). The central cage is depicted in green, the six axial cages in blue and the six equatorial cages in red.

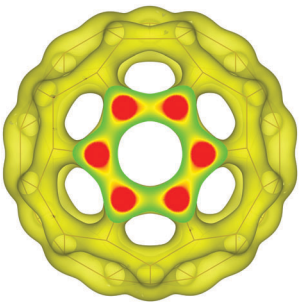

Fig. 2 Cut of the calculated electron density of C_{60} in the plane of one of the hexagonal rings. Red-to-yellow-to-green represents decreasing density. Note the greater density in the center of the 6 : 6 bonds relative to that in the center of the 6 : 5 bonds. The pentagonal and hexagonal faces are relatively electron-deficient as well.

closest-contact interactions involve 6 : 6 bonds positioned above hexagonal rings rather than above pentagonal ones. Analogous to the P orientation, the six NN cages that interact with a 6 : 6 bond from the central cage are located equatorially and the six that interact with a hexagonal ring from the central cage are located axially. In both the P and H orientations the six equatorial cages transform into one another by the operations of S_6, as do the six axial cages. The relevant cage-center coordinates and cage-orientational parameters are given in Tables S4 and S5 of the ESI.† Note, again, that we have chosen the 13-cage fragment to be oriented w.r.t. the SF axis system such that the C_3 symmetry axis of the S_6 point group lies along the SF (1,1,1) direction.

2.2.2 The electron density of C_{60} cages. The electron density of a single C_{60} molecule ($\rho^{(e)}_{cage}$) was computed *via* a first-principles DFT calculation using NWchem software[45] with a cc-PVDZ atom-centered basis set. (The C nuclear positions that were assumed for these calculations are given in Table S3 of the ESI.†) We employed an optimally tuned range-separated hybrid functional,[46,47] in which the short- and long-range portions of the exchange interaction are described by the local density approximation and non-local Fock exchange, respectively. We used a range-separation parameter of 0.21 Bohr^{-1} that enforces the ionization-potential theorem and minimizes erroneous orbital delocalization of common DFT functionals.[48,49] For the subsequent analysis, the electron density was represented on a real-space, three-dimensional grid of $N_{grid} = (601)^3$ points with equidistant 1D spacing of 0.037795 Bohr (0.02 Å).

Fig. 2 shows a cut of the calculated electron density in the plane of one of the six-membered rings. Around the ring 6 : 6 and 6 : 5 CC bonds alternate with one another. The figure shows that the electron density at the center of the 6 : 6 bonds is greater than that at the center of the 6 : 5 bonds, confirming that the former are indeed relatively electron-rich and the latter electron-poor. One can get a semi-quantitative sense of the magnitude of the charge-distribution anisotropy that this corresponds to by computing from the DFT results the first nonzero molecular moments of C_{60}, which correspond to $l = 6$. If one then compares these DFT moments with ones computed for a C_{60} point-charge model in which negative point charges ($-\delta e$) are located at the thirty 6 : 6 bond centers and positive point charges ($+2.5\delta e$) are located at the twelve pentagon centers, one finds that $\delta = 0.03$ produces a close match.

2.2.3 Evaluation of $I^{(2)}_m$. With the NN–cage positions set and the charge density for each cage determined, eqn (3) was evaluated as follows for $l = 2$ for both the P and H orientations. First, the contribution to each $I^{(2)}_m$ from one of the axial cages – "cage 1" – was computed. This was done by first translating (through vector $\mathbf{T}$) and rotating (rotation matrix $\hat{R}$) the C_{60} nuclear positions and the corresponding grid from the DFT calculation so as to make them coincide with the position of cage 1 in the relevant 13-cage unit. Any given grid point, i, given by position vector $\mathbf{d}_i$ w.r.t. a cartesian axis system fixed to the individual C_{60} cage, acquires by this translation + rotation a position vector $\mathbf{r}_i$ w.r.t. the SF axis system such that

$$\mathbf{r}_i = \mathbf{T} + \hat{R}\mathbf{d}_i. \tag{7}$$

Similarly, any given C nucleus, having position vector $\mathbf{D}_i$ w.r.t. the cage-fixed axes, acquires the SF position vector

$$\mathbf{R}_i = \mathbf{T} + \hat{R}\mathbf{D}_i. \tag{8}$$

We then computed the following:

$$I^{(2)}_m(\text{cage 1}) \simeq \sum_{i=1}^{N_{grid}} \frac{\rho^{(e)}_{cage}(\mathbf{d}_i) C^{(2)}_m(\hat{r}_i)}{r_i^3} \delta V + \sum_{i=1}^{60} \frac{6 C^{(2)}_m(\hat{R}_i)}{R_i^3}, \tag{9}$$

where $\delta V = (0.037795)^3$ Bohr^3, and the factor of 6 in the second summation comes from the individual nuclear charges. An evaluation of eqn (9) nominally gives the full contribution from cage 1 to $I^{(2)}_m$. However, because the cubic grid on which $\rho^{(e)}_{cage}$ is represented does not have the I_h symmetry of C_{60}, we have computed eqn (9) for all sixty symmetrically equivalent orientations of cage 1 (sixty different $\hat{R}$) obtained by rotating the cage through all the proper rotations of the I_h point group and have averaged the results so as to minimize any orientation anomalies due to this symmetry mismatch. We label these orientation-averaged contributions $\bar{I}^{(2)}_m$(cage 1). To obtain the contribution of all six of the axial cages to $I^{(2)}_m$ we exploit symmetry. If one labels the cage to which cage 1 is transformed by rotation by $-2\pi/3$ about the (1,1,1) SF axis as cage 2, and that to which cage 1 is transformed by rotation by $+2\pi/3$ about (1,1,1) as cage 3,

then one can show that the orientation-averaged contributions of cage 2 plus cage 3 to the $I_m^{(2)}$ are given by

$$\bar{I}_m^{(2)}(\text{cage 2}) + \bar{I}_m^{(2)}(\text{cage 3}) = \sum_{m'=-2}^{2} \left(B^*_{m,m'} + B_{m',m}\right)\bar{I}_{m'}^{(2)}(\text{cage 1}). \tag{10}$$

($B_{m,m'}$ are given in Section 3.2 of the ESI.†) Similarly, if one labels as 4, 5, and 6 the cages into which cages 1, 2 and 3 transform, respectively, by inversion through the SF origin, then

$$\sum_{k=4}^{6} \bar{I}_m^{(2)}(\text{cage } k) = \sum_{k=1}^{3} \bar{I}_m^{(2)}(\text{cage } k), \tag{11}$$

where we have used the invariance of $I_m^{(2)}$ to inversion (see Section 3.1 of the ESI†). Hence, the full axial-cage contribution (cages 1 to 6) to $I_m^{(2)}$ is given by

$$I_m^{(2)}(\text{axial}) = \sum_{m'=-2}^{2} 2\left[\delta_{m,m'} + B^*_{m,m'} + B_{m',m}\right]\bar{I}_{m'}^{(2)}(\text{cage 1}). \tag{12}$$

Finally, an exactly analogous procedure can be applied to obtain the contributions from the six equatorial cages to $I_m^{(2)}$. One computes the analog to eqn (9) for all 60 equivalent orientations of a C_{60} cage in one of the equatorial positions – "cage 7" – and averages the results to get the $\bar{I}_m^{(2)}$(cage 7). One then makes use of the transformation properties due to rotation and inversion of these quantities to obtain the contributions from the other five equatorial cages. Combining these contributions to eqn (12) one has the final result

$$I_m^{(2)} = \sum_{m'=-2}^{2} 2\left[\delta_{m,m'} + B^*_{m,m'} + B_{m',m}\right]\left[\bar{I}_{m'}^{(2)}(\text{cage 1}) + \bar{I}_{m'}^{(2)}(\text{cage 7})\right]. \tag{13}$$

By this procedure we compute for both the P orientation and the H orientation

$$[I_m^{(2)}] = A[i,(-1+i),0,(1+i),-i]; \quad m = -2,\ldots,+2. \tag{14}$$

For the P orientation $A = 6.809 \times 10^{-6}$ a.u. For the H orientation $A = -2.307 \times 10^{-7}$ a.u. Note that eqn (14) conforms to what one expects given the S_6 symmetry of both 13-cage units (Section 3.3 of the ESI†). Note also that the internal moments for the P orientation are more than an order-of-magnitude larger than, and of opposite sign from, those for the H orientation. This difference is largely due to the different contributions of the equatorial NN cages to $I_m^{(2)}$ in the two cases. In the P orientation, the equatorial contributions (corresponding to pentagon "donation" from the NN cages) are about a factor of three greater than the axial ones, and they add constructively to the latter. In contrast, the equatorial contributions in the H orientation (corresponding to hexagon "donation" from the NN cages) are close in magnitude to the axial ones, and they add destructively to them. The greater equatorial effect in the P case can be rationalized by noting that each P equatorial cage interacts with the central cage *via* five electron-deficient (6 : 5) CC bonds, whereas each H equatorial cage does so *via* three electron-deficient (6 : 5) and three electron-rich (6 : 6) CC bonds.

2.3 The molecular moments, $Q_m^{(2)}$

To quantify $Q_m^{(2)}$ we look first to literature values for the quadrupole moments of the molecules relative to a BF frame. For H_2 and HF, with the BF frame defined such that the origin is at the c.m. of the molecule and z is along the internuclear axis, the only nonzero values correspond to $m = 0$. Literature values for these are 0.499 a.u. (H_2)[50] and 1.756 a.u. (HF).[51] For H_2O, with its cartesian BF frame defined such that the origin is at the molecule's c.m., the z axis is along the bisector of $\angle$HOH pointing toward the O nucleus, and the x axis is in the molecular plane, the BF moments corresponding to $m = 0,\pm 2$ are nonzero. We use the following values, computed from data in Table II of Akin-Ojo and Szalewicz:[52] $Q_0^{\text{BF}} = -0.09973$ a.u. and $Q_{\pm 2}^{\text{BF}} = 1.53843$ a.u.

The molecular moments that appear in V_{quad} [see eqn (6)] have components that are referred to the SF frame. Hence, they can depend not only on the BF quadrupole components but also on the location of the BF frame w.r.t. the SF frame – *i.e.*, on R and ω. One can show that

$$Q_m^{(2)}(\mathbf{R},\omega) = \sum_q \left[D^{(2)}_{m,q}(\omega)\right]^* Q_q^{\text{BF}} + (-1)^m\sqrt{40\pi}\mu R \times \sum_{m',m''} \begin{pmatrix} 1 & 1 & 2 \\ m' & m'' & -m \end{pmatrix} Y_{1,m'}(\Theta,\Phi)\left[D^{(1)}_{m'',0}(\omega)\right]^*, \tag{15}$$

where (R,Θ,Φ) are the spherical coordinates associated with $\mathbf{R}$, and $\mu\hat{z} = \vec{\mu}$ is the electric-dipole vector of M, taken to lie along the BF z axis (μ can be positive or negative depending on the choice of the BF axes). Since H_2 has no dipole moment, only the $\mathbf{R}$-independent first term in eqn (15) survives for that species. However, H_2O and HF do have nonzero dipoles, and their SF quadrupole components do depend on $\mathbf{R}$. In applying eqn (15) to H_2O we use one of two values of μ: $\mu = -0.737196$ a.u., an isolated H_2O value computed from data in Table II of Akin-Ojo and Szalewicz,[52] or $\mu = -0.2$ a.u., a screened dipole value taken from Meier *et al.*[53] For HF, since we only subject the level structure splittings in HF@C_{60} to a first-order perturbation-theory analysis, there is no need (see Section 4.1 of the ESI†) to evaluate the second term on the rhs of eqn (15).

2.4 Perturbation-theory calculations of TR level splittings

Excellent estimates for some of the TR level splittings that arise from M–NN quadrupolar couplings can be obtained without full 5D or 6D solution of the TR Schrödinger equation by using degenerate first-order perturbation theory. One treats that part of the M@C_{60} TR Hamiltonian apart from V_{quad} as the zeroth-order Hamiltonian and V_{quad} as the perturbation. For M = H_2 and H_2O (and, we assume, for M = HF, too) the lowest-energy zeroth-order states in this scheme are very well approximated as translation/rotation product functions of the form[12,15]

$$|T_0\rangle|j,m_j\rangle \text{ (for } H_2 \text{ and HF)}, \quad |T_0\rangle|j_{k_a k_c},m_j\rangle \text{ for } H_2O, \tag{16}$$

where $|T_0\rangle$ is an **R**-dependent function corresponding to the ground state of the c.m. translational mode, $|j,m_j\rangle$ is a linear rigid-rotor rotational eigenstate and $|j_{k_a}k_b,m_j\rangle$ is a rigid-asymmetric-top rotational eigenstate. The first-order, quadrupole-induced splitting of a level corresponding to a given j or $j_{k_a}k_b$ can be computed by evaluating the matrix elements of $V_{\rm quad}$ within the degenerate set of states corresponding to the $(2j + 1)$ possible values of m_j, and then diagonalizing the matrix. By making use of eqn (15) one can obtain analytic expressions for the level splittings.

We have applied this approach to the calculation of the splittings of $j = 1$ levels in the three M@C_{60} species considered herein, as it is just these splittings that have been measured by experiment. One can show (Section 4 of the ESI†) that the three states corresponding to such a level are always split by $V_{\rm quad}$ into a doubly-degenerate level ($g = 2$) and a nondegenerate one ($g = 1$), with the splitting given by

$$\Delta_{\rm PT} \equiv E(g = 2) - E(g = 1) = 3Af(Q^{\rm BF}), \tag{17}$$

where A is the internal-moment quantity that appears in eqn (14) and $f(Q^{\rm BF})$ is solely a function of M's BF quadrupole tensor with the functional form that depends on the specific nature of the $j = 1$ rotational level. For both H_2 and HF

$$f(Q^{\rm BF}) = \frac{\sqrt{6}}{5}Q_0^{\rm BF}, \tag{18}$$

while for the $|1_{01}\rangle$ state of H_2O@C_{60}

$$f(Q^{\rm BF}) = \frac{3}{5}\left[-\sqrt{\frac{1}{6}}Q_0^{\rm BF} + \frac{1}{2}(Q_2^{\rm BF} + Q_{-2}^{\rm BF})\right]. \tag{19}$$

2.5 Variational calculations of TR level structures

Going beyond PT, one can diagonalize eqn (1) using variational methods. We have solved for the low-energy eigenstates of these Hamiltonians by using Chebyshev[54] filter diagonalization,[55] an iterative method that requires repeated Hamiltonian-on-state-vector ($\hat{H}|\psi\rangle$) operations. For H_2 we used a product basis consisting of functions of the form $|n,l,m_l\rangle\ |j,m_j\rangle$, where $|n,l,m_l\rangle$ are three-dimensional isotropic harmonic-oscillator eigenfunctions and $|j,m_j\rangle$ are linear-rigid-rotor eigenfunctions. (See Section 2.1.1 of the ESI† for full details on the basis.) Based on this the matrix elements of $\hat{T}$ have analytical expressions, and the required $\hat{T}|\psi\rangle$ operations are readily computed. To effect the operation of the potential-energy operator on $|\psi\rangle$ we transformed the state vector into a 5D grid representation $(R_a,(\cos\Theta)_b,\Phi_c,(\cos\theta)_d,\phi_e) \equiv (a,b,c,d,e)$. Here the $(R_a,(\cos\Theta)_b,\Phi_c) \equiv \mathbf{R}_{a,b,c}$ portion of the grid spans the spherical-polar coordinates (R,Θ,Φ) associated with **R**. R_a are Gauss-associated-Laguerre quadrature points, $(\cos\Theta)_b$ are Gauss–Legendre quadrature points, and Φ_c constitute a Fourier grid. The $((\cos\theta)_d,\phi_e) \equiv \omega_{d,e}$ portion of the grid spans the two rotation angles ω. $(\cos\theta)_d$ are Gauss–Legendre quadrature points and ϕ_e constitute a Fourier grid. (See Section 2.1.2 of the ESI† for full details on the 5D grid.) After transformation of $|\psi\rangle$ to the grid, we then multiplied the state vector at each grid point by the value of the potential energy at that grid point:

$$V(a,b,c,d,e) \equiv V_{\rm LJ}(R_{a,b,c},\omega_{d,e}) + \sum_{m=-2}^{2}(-1)^m I_{-m}^{(2)}Q_m^{(2)}(\mathbf{R}_{a,b,c},\omega_{d,e}). \tag{20}$$

Finally, the resulting vector was transformed back into the $|n,l,m_l\rangle|j,m_j\rangle$ representation.

For H_2O@C_{60} the methodology employed was analogous to that used for H_2@C_{60} except that the rotational part of the basis consisted of normalized Wigner rotation matrix elements

$$|j,m_j,k\rangle = \sqrt{2j+1/8\pi^2}\left[D_{m_j,k}^{(j)}(\omega)\right]^* \tag{21}$$

rather than $|j,m_j\rangle$, and the rotational-angle portion of the (now) 6D grid covered the three Euler angle coordinates $\omega \equiv (\phi,\theta,\chi)$ with Gauss–Legendre quadrature points $(\cos\theta)_d$, and Fourier grid points ϕ_e and χ_f. (See Section 2.2 of the ESI† for details on the basis and grid parameters employed for this species.)

3 Results and discussion

Table 1 shows the splittings of the ground states of *ortho*-H_2, *ortho*-H_2O and the $j = 1$ level of HF induced by the quadrupolar model of M–NN electrostatic interactions in eqn (6), calculated for the P and H orientations variationally and by PT (for HF, only PT calculations could be performed since a 5D intermolecular PES is not available for HF@C_{60}).

One immediately notes that the splittings calculated, both variationally and by the first-order PT, for all three species in the P orientation are in excellent agreement with the experimental results for M@C_{60}(s), that are also given in Table 1. Another striking feature of the theoretical results shown in Table 1 is that for the three M@C_{60}(s) systems considered, the $j = 1$ (or $j_{k_a k_c} = 1_{01}$, for H_2O) splittings calculated for the H orientation are about 30 times smaller than those obtained for the P orientation, and their pattern is reversed, *i.e.*, 2 : 1.

Table 1 Perturbation-theory-calculated ($\Delta_{\rm PT}$) and variationally calculated ($\Delta_{\rm var}$) quadrupole-induced splittings (in cm^{-1}) of the $j = 1$ levels of the endohedral H_2 and HF, and the $j_{k_a k_c} = 1_{01}$ level of H_2O, for the P and H orientations. They are compared with the corresponding level splittings ($\Delta_{\rm obs}$) observed in M@C_{60}(s) samples. $f(Q^{\rm BF})$ functions (in a.u.) are defined in eqn (18) for H_2 and HF, and in eqn (19) for H_2O

M	$f(Q^{\rm BF})$	P/H	$\Delta_{\rm PT}$	$\Delta_{\rm var}$	$\Delta_{\rm obs}$
H_2	0.2445	P[a]	1.096	1.096	1.09 ± 0.1[b]
		H	−0.037	−0.037	—
HF	0.8603	P	3.86	—	3.9[c]
		H	−0.13	—	—
H_2O	0.9475	P	4.25	4.15/4.22[d]	4.19[e]
		H	−0.14	−0.14	—

[a] All P splittings were calculated for $A = 6.809 \times 10^{-6}$ a.u. All H splittings were calculated for $A = -2.307 \times 10^{-7}$ a.u. [b] From Mamone *et al.*[33] [c] From Krachmalnicoff *et al.*[8] [d] First value is for $\mu = -0.737916$ and the second for $\mu = -0.2$ a.u. [e] From Goh *et al.*[35]

This reflects the fact noted earlier in the paper, that for the H orientation, the internal-moment quantity A that appears in eqn (14), and enters in the PT expression for the level splitting in eqn (17), is more than an order of magnitude smaller than, and has the opposite sign from, that for the P orientation. Important insight gained from the above is that the observed TR level splittings in M@C_{60}(s) systems due to symmetry-breaking come almost exclusively from the P orientation, while the contribution from the H orientation is negligible.

In addition, for all three systems, the calculations predict that, for the P orientation, the three-fold degenerate j = 1 (or $j_{k_a k_c}$ = 1_{01}, for H_2O) level of M is split into a non-degenerate lower-energy level and a doubly degenerate higher energy level. This is in agreement with the 1 : 2 splitting pattern observed in H_2@C_{60}(s)[33] and H_2O@C_{60}(s).[34–36] For HF@C_{60}(s), the j = 1 level splitting pattern has not been reported.[8]

All these calculations have employed the values of the quadrupole moments determined for the isolated H_2, HF, and H_2O, respectively. A question can be raised as to whether these values are appropriate when the molecules are inside C_{60}, since the fullerene cage is known to reduce the dipole moments of the endohedral H_2O[53,56] and HF[8] to about 25% of those for the isolated molecules. No information, experimental or theoretical, is available about the quadrupole moments of molecules in C_{60} at present. However, it is easy to check that the ratio of the experimental splittings of the j = 1 levels of HF and *ortho*-H_2, 3.9/1.09 = 3.58, mirrors the ratio of the BF quadrupole moments of these two molecules, 1.756/0.499 = 3.52. In the same vein, the ratio of the splittings measured for the 1_{01} level of *ortho*-H_2O and the j = 1 level of *ortho*-H_2, 4.19/1.09 = 3.84, is very close to the ratio of the $f(Q^{BF})$ functions (that depend solely on the molecules' BF quadrupole tensors) of the two molecules in eqn (18) and (19), respectively, 0.9475/0.2445 = 3.875. Such direct proportionality between the level splittings of the three endohedral molecules and their respective quadrupole moments constitutes compelling evidence that the quadrupolar M–NN interaction is the predominant source of the symmetry breaking in these M@C_{60}(s) systems.

Moreover, for all three M@C_{60} systems considered, our calculations, which are free from adjustable parameters, reproduce the experimental results using the gas-phase values of the quadrupole moments of the guest molecules (H_2, HF, H_2O). This strongly suggests that the quadrupole moments of molecules inside C_{60} are not significantly affected by the encapsulation. At present we do not have a rigorous explanation for this intriguing observation, though it is not unthinkable that the quadrupole polarizability of C_{60} might be considerably less than the dipole polarizability. We regard this as a ripe topic for further investigation.

4 Conclusions

We have investigated the origin of the symmetry breaking in the endofullerenes M@C_{60}(s) (M = H_2, HF, H_2O) that manifests in the splittings of the three-fold degenerate ground states of the endohedral *ortho*-H_2, *ortho*-H_2O and the j = 1 level of HF, ranging from about 1 cm^{-1} for H_2 to about 4 cm^{-1} for HF and H_2O. For this purpose, we have developed a model focusing on a fragment of solid C_{60}, in which twelve nearest-neighbor (NN) cages surround the central cage, and all the cages have either the P or the H orientation. Only the central cage is occupied by the guest molecule M, while the twelve NN cages are empty.

The proposition at the heart of the model is that the symmetry breaking in M@C_{60}(s) arises predominantly from the electrostatic interactions between the charge densities on the NN C_{60} cages and those on M, and that retaining just its leading quadrupole terms suffices to quantitatively account for the manifestations considered in this study. The splittings of TR levels of interest for M inside the central C_{60} and under the quadrupolar interaction with the twelve NN cages have been computed for the P and H orientations by means of variational calculations in 5D (H_2) and 6D (H_2O), as well as by the first-order PT (H_2, HF, and H_2O). The two methods yield very similar results.

For the P orientation, the splittings calculated in this way for the ground states of *ortho*-H_2, *ortho*-H_2O and the j = 1 level of HF agree extremely well, to within the experimental error bars, with those measured for the corresponding M@C_{60}(s) systems. In addition, the calculations yield the 1 : 2 splitting patterns observed in the experiments. It should be emphasized here that the M–NN electrostatic interactions contain no adjustable parameters. The electron density on the NN cages results from a first-principles DFT calculation, and the charge density on M is related to its BF quadrupole moments reported in the literature. Therefore, the ability of the model to reproduce the available experimental results with such a high accuracy provides a strong argument in favor of its central tenet that the quadrupolar M–NN interaction is the main mechanism for the symmetry breaking in the M@C_{60}(s) species considered, both for endohedral molecules without (H_2) and with (H_2O and HF) permanent dipole moments. In addition, as predicted by the model, the experimental splittings of the levels considered scale directly with the magnitude of the quadrupole moments of the endohedral molecules.

A very surprising result of these calculations is that for the H orientation the symmetry-induced splittings are about a factor of 30 smaller than the corresponding ones in the P orientation. This striking difference can be traced back to an internal-moment quantity that in the H orientation is over an order of magnitude smaller than in the P orientation. It follows, therefore, that the splittings of the TR levels observed in the M@C_{60}(s) systems of interest are associated with the P orientation, the contribution from the H orientation being negligible.

In order to appreciate fully the implications of quantitative accuracy of the quadrupolar model introduced in this study, it is worth reminding how simple conceptually it actually is. A fragment consisting of just thirteen C_{60} molecules is considered, the individual cages are treated as rigid, and the latter are assumed to have icosahedral symmetry. A single guest molecule M resides in the central cage, and experiences the quadrupolar interaction with the twelve NN cages that are unoccupied. And yet, the results of this minimal, stripped-down model are in quantitative agreement with the experimental values.

This leaves little room for the contributions from other mechanisms for symmetry breaking in M@C_{60}(s) that have been implicated, *e.g.*, distortion of the C_{60} geometry caused by the interaction with the endohedral M and, when M has a permanent electric dipole moment (HF, H_2O), emergence of dipole-ordered phases, *i.e.*, ferroelectricity.[34,57] They are likely to be of minor significance.

Conflicts of interest

There are no conflicts of interest to declare.

Acknowledgements

Z. B., D. N., and S. F. are grateful to the National Science Foundation for its partial support of this research through Grants CHE-1566085, DMR/BSF-1611382, and CHE-1565961, respectively.

References

1 M. H. Levitt, *Philos. Trans. R. Soc., A*, 2013, **371**, 20120429.
2 K. Komatsu, M. Murata and Y. Murata, *Science*, 2005, **307**, 238.
3 M. Murata, Y. Murata and K. Komatsu, *J. Am. Chem. Soc.*, 2006, **128**, 8024.
4 Y. Rubin, *Chem. – Eur. J.*, 1997, **3**, 1009.
5 Y. Rubin, *Top. Curr. Chem.*, 1999, **199**, 67.
6 Y. Rubin, T. Jarrosson, G. W. Wang, M. D. Bartberger, K. N. Houk, G. Schick, M. Saunders and R. J. Cross, *Angew. Chem., Int. Ed.*, 2001, **40**, 1543.
7 K. Kurotobi and Y. Murata, *Science*, 2011, **333**, 613.
8 A. Krachmalnicoff, R. Bounds, S. Mamone, S. Alom, M. Concistrè, B. Meier, K. Kouřil, M. E. Light, M. R. Johnson, S. Rols, A. J. Horsewill, A. Shugai, U. Nagel, T. Rõõm, M. Carravetta, M. Levitt and R. J. Whitby, *Nat. Chem.*, 2016, **8**, 953.
9 P. R. Bunker and P. Jensen, *Molecular Symmetry and Spectroscopy, E-book edition*, NRC Research Press, Ottawa, Ontario, Canada, 2006.
10 S. Mamone, J. Y. C. Chen, R. Bhattacharyya, M. H. Levitt, R. G. Lawler, A. J. Horsewill, T. Rõõm, Z. Bačić and N. J. Turro, *Coord. Chem. Rev.*, 2011, **255**, 938.
11 M. Xu, F. Sebastianelli, Z. Bačić, R. Lawler and N. J. Turro, *J. Chem. Phys.*, 2008, **128**, 011101.
12 M. Xu, F. Sebastianelli, Z. Bačić, R. Lawler and N. J. Turro, *J. Chem. Phys.*, 2008, **129**, 064313.
13 M. Xu, F. Sebastianelli, B. R. Gibbons, Z. Bačić, R. Lawler and N. J. Turro, *J. Chem. Phys.*, 2009, **130**, 224306.
14 S. Mamone, M. Ge, D. Hüvonen, U. Nagel, A. Danquigny, F. Cuda, M. C. Grossel, Y. Murata, K. Komatsu, M. H. Levitt, T. Rõõm and M. Carravetta, *J. Chem. Phys.*, 2009, **130**, 081103.
15 P. M. Felker and Z. Bačić, *J. Chem. Phys.*, 2016, **145**, 084310.
16 M. Xu, S. Ye, R. Lawler, N. J. Turro and Z. Bačić, *Philos. Trans. R. Soc., A*, 2013, **371**, 20110630.
17 M. Xu, S. Ye, A. Powers, R. Lawler, N. J. Turro and Z. Bačić, *J. Chem. Phys.*, 2013, **139**, 064309.
18 A. J. Horsewill, S. Rols, M. R. Johnson, Y. Murata, M. Murata, K. Komatsu, M. Carravetta, S. Mamone, M. H. Levitt, J. Y. C. Chen, J. A. Johnson, X. Lei and N. J. Turro, *Phys. Rev. B: Condens. Matter Mater. Phys.*, 2010, **82**, 081410(R).
19 A. J. Horsewill, K. S. Panesar, S. Rols, J. Ollivier, M. R. Johnson, M. Carravetta, S. Mamone, M. H. Levitt, Y. Murata, K. Komatsu, J. Y. C. Chen, J. A. Johnson, X. Lei and N. J. Turro, *Phys. Rev. B: Condens. Matter Mater. Phys.*, 2012, **85**, 205440.
20 A. J. Horsewill, K. Goh, S. Rols, J. Ollivier, M. R. Johnson, M. H. Levitt, M. Carravetta, S. Mamone, Y. Murata, J. Y. C. Chen, J. A. Johnson, X. Lei and N. J. Turro, *Philos. Trans. R. Soc., A*, 2013, **371**, 20110627.
21 S. Mamone, M. Jiménez-Ruiz, M. R. Johnson, S. Rols and A. J. Horsewill, *Phys. Chem. Chem. Phys.*, 2016, **18**, 29369.
22 M. Ge, U. Nagel, D. Hüvonen, T. Rõõm, S. Mamone, M. H. Levitt, M. Carravetta, Y. Murata, K. Komatsu, J. Y. C. Chen and N. J. Turro, *J. Chem. Phys.*, 2011, **134**, 054507.
23 M. Ge, U. Nagel, D. Hüvonen, T. Rõõm, S. Mamone, M. H. Levitt, M. Carravetta, Y. Murata, K. Komatsu, X. Lei and N. J. Turro, *J. Chem. Phys.*, 2011, **135**, 114511.
24 T. Rõõm, L. Peedu, M. Ge, D. Hüvonen, U. Nagel, S. Ye, M. Xu, Z. Bačić, S. Mamone, M. Levitt, M. Carravetta, J. Y. C. Chen, X. Lei, N. J. Turro, Y. Murata and K. Komatsu, *Philos. Trans. R. Soc., A*, 2013, **371**, 20110631.
25 P. M. Felker and Z. Bačić, *J. Chem. Phys.*, 2016, **144**, 201101.
26 M. Xu, L. Ulivi, M. Celli, D. Colognesi and Z. Bačić, *Phys. Rev. B: Condens. Matter Mater. Phys.*, 2011, **83**, 241403(R).
27 M. Xu and Z. Bačić, *Phys. Rev. B: Condens. Matter Mater. Phys.*, 2011, **84**, 195445.
28 M. Xu, L. Ulivi, M. Celli, D. Colognesi and Z. Bačić, *Chem. Phys. Lett.*, 2013, **563**, 1.
29 M. Xu, M. Jiménez-Ruiz, M. R. Johnson, S. Rols, S. Ye, M. Carravetta, M. S. Denning, X. Lei, Z. Bačić and A. J. Horsewill, *Phys. Rev. Lett.*, 2014, **113**, 123001.
30 M. Xu, S. Ye and Z. Bačić, *J. Phys. Chem. Lett.*, 2015, **6**, 3721.
31 B. Poirier, *J. Chem. Phys.*, 2015, **143**, 101104.
32 Y. Kohama, T. Rachi, J. Jing, Z. Li, J. Tang, R. Kumashiro, S. Izumisawa, H. Kawaji, T. Atake, H. Sawa, Y. Murata, K. Komatsu and K. Tanigaki, *Phys. Rev. Lett.*, 2009, **103**, 073001.
33 S. Mamone, M. R. Johnson, J. Ollivier, S. Rols, M. H. Levitt and A. J. Horsewill, *Phys. Chem. Chem. Phys.*, 2016, **18**, 1998.
34 C. Beduz, M. Carravetta, J. Y. C. Chen, M. Concistre, M. Denning, M. Frunzi, A. J. Horsewill, O. G. Johannessenn, R. Lawler, X. Lei, M. H. Levitt, Y. Li, S. Mamone, Y. Murata, U. Nagel, T. Nishida, J. Ollivier, S. Rols, T. Rõõm, R. Sarkar, N. J. Turro and Y. Yang, *Proc. Natl. Acad. Sci. U. S. A.*, 2012, **109**, 12894.
35 K. S. K. Goh, M. Jiménez-Ruiz, M. R. Johnson, S. Rols, J. Ollivier, M. S. Denning, S. Mamone, M. H. Levitt, X. Lei, Y. Li, N. J. Turro, Y. Murata and A. J. Horsewill, *Phys. Chem. Chem. Phys.*, 2014, **16**, 21330.
36 A. J. Horsewill, A. J. Horsewill has informed us that the observed 1_{01} splitting in $H_2O@C_{60}$ is such that the lower

energy level is nondegenerate and the upper one is doubly degenerate. Due to a misprint, the opposite ordering was erroneously reported in Goh, *et al.*[35].

37 P. A. Heiney, J. E. Fischer, A. R. McGhie, W. J. Romanow, A. M. Denenstein, J. P. McCauley, Jr., A. B. Smith, III and D. Cox, *Phys. Rev. Lett.*, 1991, **66**, 2911.

38 W. I. F. David, R. M. Ibberson, T. J. S. Dennis, J. P. Hare and K. Prassides, *Europhys. Lett.*, 1992, **18**, 219.

39 W. I. F. David, R. M. Ibberson, J. C. Matthewman, K. Prassides, T. J. S. Dennis, J. P. Hare, H. W. Kroto, R. Taylor and D. R. M. Walton, *Nature*, 1991, **353**, 147.

40 M. S. Dresselhaus, G. Dresselhaus and P. Eklund, *Science of Fullerenes and Carbon Nanotubes*, Academic Press, 1995.

41 R. N. Zare, *Angular Momentum: Understanding Spatial Aspects in Chemistry and Physics*, Wiley-Intersience, New York, 1988.

42 R. Sachidanandam and A. B. Harris, *Phys. Rev. Lett.*, 1991, **67**, 1467.

43 A. B. Harris and R. Sachidanandam, *Phys. Rev. B: Condens. Matter Mater. Phys.*, 1992, **46**, 4944.

44 S. Aoyagi, N. Hoshino, T. Akutagawa, Y. Sado, R. Kitaura, H. Shinohara, K. Sugimoto, R. Zhang and Y. Murata, *Chem. Commun.*, 2014, **50**, 524.

45 M. Valiev, E. J. Bylaska, N. Govind, K. Kowalski, T. P. Straatsma, H. J. J. V. Dam, D. Wang, J. Nieplocha, E. Apra, T. L. Windus and W. A. de Jong, *Comput. Phys. Commun.*, 2010, **181**, 1477.

46 A. Savin and H.-J. Flad, *Int. J. Quantum Chem.*, 1995, **56**, 327.

47 R. Baer and D. Neuhauser, *Phys. Rev. Lett.*, 2005, **94**, 043002.

48 P. Mori-Sanchez, A. J. Cohen and W. Yang, *Phys. Rev. Lett.*, 2008, **100**, 146401.

49 L. Kronik, T. Stein, S. Refaely-Abramson and R. Baer, *J. Chem. Theory Comput.*, 2012, **8**, 1515.

50 R. LeSar and D. R. Herschbach, *J. Phys. Chem.*, 1983, **87**, 5202.

51 F. H. de Leluw and A. Dymanus, *J. Mol. Spectrosc.*, 1973, **48**, 427.

52 O. Akin-Ojo and K. Szalewicz, *J. Chem. Phys.*, 2005, **123**, 134311.

53 B. Meier, S. Mamone, M. Concistre, J. Alonso-Valdesueiro, A. Krachmalnicoff, R. J. Whitby and M. H. Levitt, *Nat. Commun.*, 2015, **6**, 8112.

54 V. A. Mandelshtam and H. S. Taylor, *J. Chem. Phys.*, 1997, **106**, 5085.

55 M. R. Wall and D. Neuhauser, *J. Chem. Phys.*, 1995, **102**, 8011.

56 B. Ensing, F. Costanzo and P. L. Silvestrelli, *J. Phys. Chem. A*, 2012, **116**, 12184.

57 J. Cioslowski and A. Nanayakkara, *Phys. Rev. Lett.*, 1992, **69**, 2871.